Detection of Hertz Frequency Multi-Harmonic Field Lines Resonances at Low-L (L∼1.2) during Van Allen Probe Perigee Passes

F. R. Lena[1,2], L. G. Ozeke[1], J. R. Wygant[3], S. Tian[3], A. W. Breneman[3] and I. R. Mann[1]

[1]Department of Physics, University of Alberta, Edmonton, Alberta, Canada.

[2]Sao Carlos School of Engineering, University of Sao Paulo, Sao Carlos, Sao Paulo, Brazil.

[3]School of Physics and Astronomy, University of Minnesota, Minneapolis, Minnesota 55455, U.S.A.

Corresponding author: L. G. Ozeke (lozeke@ualberta.ca)

Key Points:

- We present previously unreported low-L (L~1.2) Hertz frequency multi-harmonic field line resonances, observed in the electric field spectra
- The field line resonance harmonics were regularly observed by the Van Allen Probes, and have frequencies consistent with odd harmonic modes
- The observed harmonic frequencies are compared to models using empirical density profiles, offering a new diagnostic for density dynamics

Abstract

We present new and previously unreported in-situ observations of Hertz frequency multi-harmonic mode field line resonances detected by the Electric Field and Waves (EFW) instrument on-board the NASA Van Allen Probes during low-L perigee passes. Spectral analysis of the spin-plane electric field data reveals the waves in numerous perigee passes, in sequential passes of Probes A and B, and with harmonic frequency structures from ~0.5 to 3.5 Hz which vary with L-shell, altitude, and from day to day. Comparing the observations to wave models using plasma mass density values along the field line given by empirical power laws and from the International Reference Ionosphere model (IRI), we conclude the waves are standing Alfvén field line resonances, and that only odd-mode harmonics are excited. The model eigenfrequencies are strongly controlled by the density close to the apex of the field line, suggesting a new diagnostic for equatorial ionospheric density dynamics.

1. Introduction

In the Earth's magnetosphere standing Alfvén wave oscillations along the length of the field lines can occur in the form of harmonic field line resonances (FLRs) at a discrete set of eigenfrequencies. These eigenfrequencies depend on the length of the magnetic field line, as well as the magnetic field strength and plasma mass density along the field line (e.g., Chen & Hasegawa, 1974 and Southwood, 1974). The standing waves can be excited internally by unstable energetic charged particle distributions (e.g., Southwood et al. 1969, Ozeke & Mann 2001, and Zhu et al. 2020) or externally by the interaction of the solar wind with the Earth's magnetic field (e.g., Allan et al. 1986, Kivelson & Pu, 1984, Mathie & Mann, 2000). These waves have also been shown to

play an important role in the acceleration and transport of relativistic electrons in the outer radiation belt (e.g., Falthammar et al. 1965, Ozeke et al. 2020).

Early work reported the existence of auroral zone discrete field line resonances in ground-magnetometer data (e.g., Samson et al., 1971), with later work further characterizing the existence of discrete frequency field line resonances associated with discrete frequency waveguide modes in ground-based magnetometer (e.g., Mathie et al., 1999), radar (e.g., Ruohoniemi et al., 1991; Fenrich et al., 1995) and in-situ data (e.g., Rae et al., 2005). Mathie et al. (2000) and Menk et al. (1994), used the cross phase technique (e.g., Waters et al., 1995) applied to ground-based magnetometer data at high latitudes to clearly demonstrate that discrete frequency FLRs were local enhancements in the Alfvén continuum, with in-situ satellite data also showing evidence of broad-band excitation of Alfvén waves in the continuum (cf., Engebretson et al., 1986; Anderson et al., 1990) consistent with the theory of Hasegawa et al. (1983).

Typically, in-situ measurements of harmonic field line resonances from the field instruments on satellites in high altitude elliptical orbits are limited to higher L-shells (cf. Takahashi et al, 1990, for L=2-6). Similarly, ground-based magnetometer data has shown Pc3-4 field line resonances at mid-latitudes (e.g., Mathie & Mann, 2000), and at lower L-shells (e.g., Ziesolleck et al., 1993; Menk et al., 1994; from around L=1.4-2.7), with Green et al. (1993) reporting local field line resonance frequencies in ground-based magnetometer data at $L \gtrsim 1.5$ with frequencies from 66 to 84 mHz. In-situ satellites in polar low-Earth orbit (LEO), such as those from the ESA Swarm constellation, have observed Hertz frequency waves at mid and high-latitudes (e.g., Kim et al., 2018), but these are usually associated with a higher altitude driver such as the growth of electromagnetic ion cyclotron (EMIC) waves which are excited in the equatorial plane and then propagate along field lines to the ionosphere.

Here we report observations of Hertz frequency standing mode harmonic field line resonances which are observed in the electric field dynamic power spectra during low inclination perigee passes of the NASA Van Allen Probes. To our knowledge, such observations are new and previously unreported. By comparing the observed harmonic spectra to those from models, we conclude that only odd-mode standing wave harmonics are exited. There is also significant current interest in monitoring near-equatorial plasma dynamics, for example in relation to plasma bubbles (e.g., Park et al., 2015, and references therein). We discuss the potential future utility of our in-situ observations of these low-L FLRs as a new diagnostic for equatorial ionospheric plasma mass density dynamics.

2. Data and Instrumentation

The primary data used in this study comes from the two Van Allen probes orbiting at a highly elliptical, 10° inclination, geocentric orbit, originally with a perigee of ~600 km and an apogee of ~30 000 km (Kessel et. al, 2013). However, toward the end of Van Allen Probe mission the perigee was lowered to below ~300 km. The Electric Field and Waves (EFW) instrument suit used in this study, consisted of 4 sensors in the spin plane and 2 sensors perpendicular to the spin plane on tubular extendable booms, resulting in 3 electric dipoles for differential potential measurements. The equipment was designed to detected quasi-static, low frequency three-dimensional electric fields. The basic survey mode measures the electric field at 32 samples per second during the entire orbit. Experimental data shows that the equipment is sensitive to electric fields down to < 0.3 mV/m (Wygant et. al., 2013). The raw, spin-plane **E**-field used here was calculated from the potential difference between the sensors using $(V_2 - V_1)/X$ where V_1 and V_2

are the potentials from opposite sensors 1 and 2 respectively, and X is their separation length of around 100 meters. The probe's spin axis points at the sun forming an angle of ± 10.5°, with attitude maneuvers approximately every 21 days (Dipak et.al., 2010).

The EFW data is taken at an average data rate of 12 kbps (Kristin et. al., 2016) the datasets are publically available in 4 different preprocessed formats (Level 1 - raw - to Level 4 - fully processed) in ".cdf" files. The data presented here is from the EFW Level 2 16 samples per second electric field probe sensor potentials in day-long datasets. In the data presented here a high-pass filter was applied to remove the slow-spin tone caused by the probes' ~11 seconds spin period and very low frequency elements. An FFT was used to produce dynamic spectrograms, which highlight the temporal evolution of the observed wave frequencies.

No clear and contemporaneous magnetic signatures of the waves were detected using The Electric and Magnetic Field Instrument Suite and Integrated Science (EMFISIS) magnetic search coils (MSC) data. This could be due to the frequency response of the MSC instruments which are optimized for frequencies from 10 Hz to 12 kHz, and the frequency response drops off by a factor of 20 from 10 Hz to 1 Hz. In addition, the Doppler effect of the fast-moving spacecraft close to perigee produces additional strong magnetic field signals making detection of the background waves difficult.

The electric field spectrograms during 72 and 75 perigee passes of probes A and B, respectively, occurring during January 2018 were manually analyzed. In the perigee pass data analyzed, Hertz frequency waves were a common occurrence both during and outside of this interval. To illustrate this, some additional example spectrograms from later epochs after January 2018 are presented in the supporting material in Figures S2 and S3. Here we select an example electric field spectrogram which occurred during the perigee pass of probe B from 16:22 to 17:22 UTC on January 1st 2018 for detailed analysis.

3. Observations

The low frequency waves present in the spectrogram during the perigee pass of probe B on January 1, 2018, from 16:22 to 17:22 UTC, clearly illustrate evidence of multiple apparently harmonic wave frequencies. In order to examine if these wave frequencies result from different harmonic modes of standing field line resonances, the observed frequencies are compared with the eigenfrequencies from a standing wave mode, determined by solving the guided Alfvén wave equation in a dipole field.

Figure 1 shows the event in detail, presenting the spectrogram as a function of L-shell and MLT in panel (a), and the altitude profile of probe B and the time series of the electric field derived from the potential difference between the electric field sensors in panel (b). Geomagnetic activity remained quiet during January 2018 with Dst never dropping below -27 nT and Kp never exceeding 4.7. Wave signatures are present in the spectrogram during this entire one-hour long dataset where the altitude of probe B varied between 622.7 km and 5937.3 km. Varying apparently harmonic wave frequencies can easily be distinguished during the in-bound perigee pass as the probe dropped below $L \lesssim 1.5$. As the probe moved inwards onto lower L-shells the observed wave frequencies increased, reaching a maximum of ~ 3.5 Hz at L=1.2. The frequency bands become less distinguishable during the outbound interval of the perigee pass, although there is evidence that they reappear again later in the outbound interval, the data suggesting that the frequencies in general decrease again as the probe moves towards higher-L.

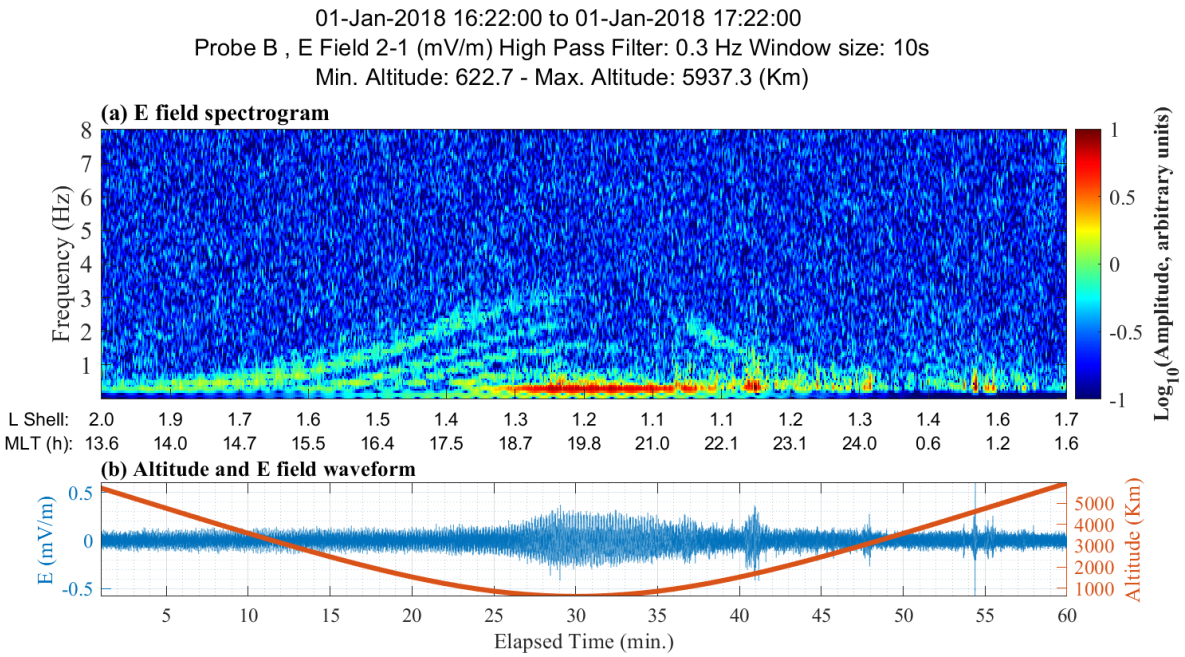

Figure 1. Panel (a) electric field spectrogram during perigee pass of probe B from 16:22 to 17:22 UTC on January 1st 2018 as a function of L-shell and MLT. Panel (b) time series of the electric field oscillations measured by the EFW instrument and altitude profile of probe B during the perigee pass.

Wave signatures similar to those shown in the spectrogram in Figure 1 can be identified during almost all perigee passes from both probes during January 2018, as shown in Figure 2 (see also supporting material Figure S1). Figure 2 consists of six different spectrogram plots of 1-hour-long perigee-centered windows. The data is from perigee passes on January 1, 3 and 6, 2018, with additional spectrograms during perigee passes on January 2, 6, 19, 14, 18, 22, 26, 30 shown in the supporting material Figure S1. The time domain waveform data was detrended by a 0.3 Hz high-pass minimum order filter to remove the strong spin tone and its harmonics generated by the probes' ~12 second spin period. The rise and fall in the wave frequencies detected during each perigee pass is similar for both probes A and B. However, more intense frequency band structures are detected on probe B making identification of the different frequencies clearer along the perigee passes of probe B.

The spectrograms were calculated using a Fast Fourier Transform (FFT) algorithm with 10-second (160 samples) long Hanning windows (Harris, 1978). The Mcllwain L-shell (Mcllwain, 1961) parameter was obtained from the probe's ephemeris data and was plotted along the spectrograms horizontal axis along with the magnetic local time (MLT). No geomagnetic storms were observed during the period of 6 days spanned by the perigee passes in Figure 2, as indicated in Figure 2 panel (g).

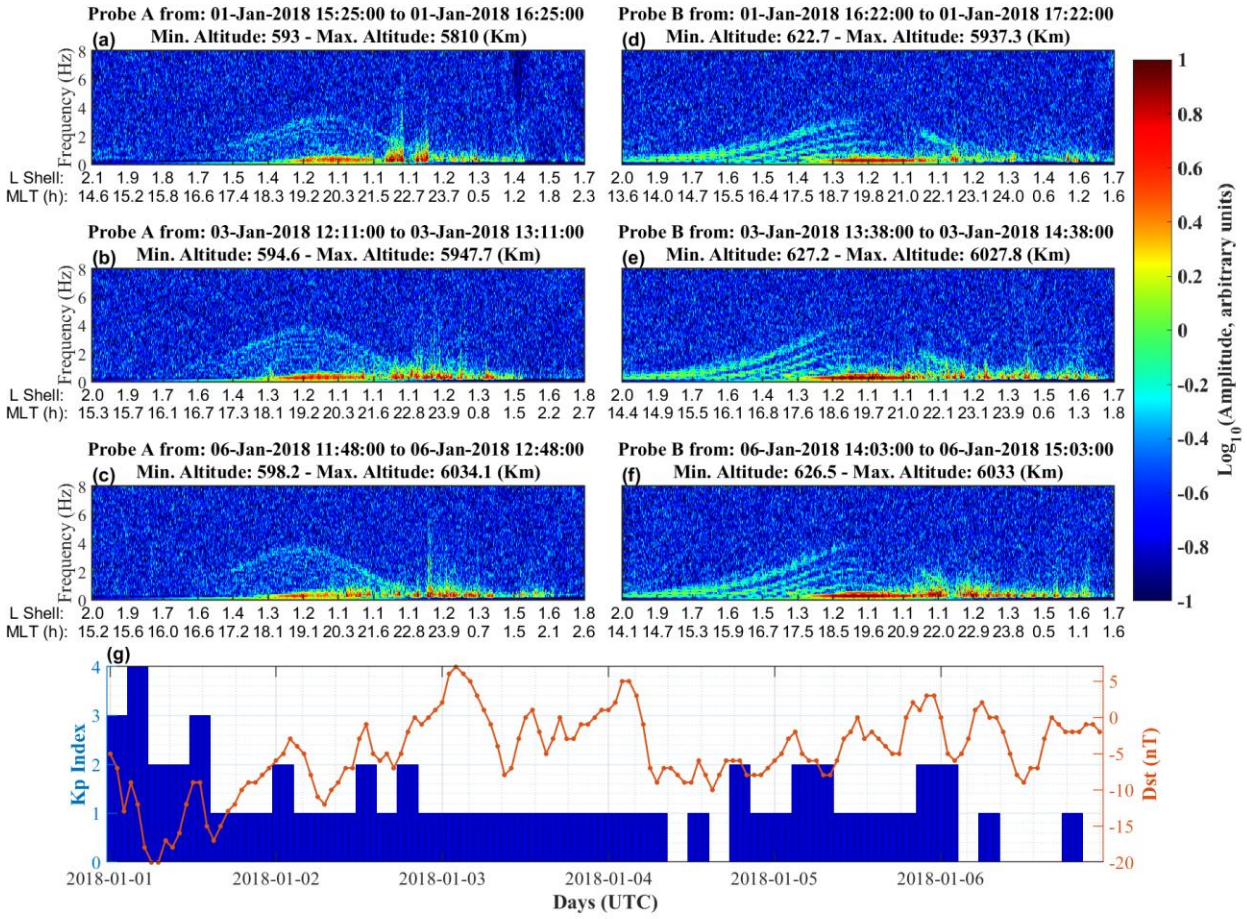

Figure 2. Panels (a) to (f) indicate the electric field spectrogram measured along perigee passes of probes A and B from January 1st to January 6th 2018. Panel (g) the time evolution of geomagnetic indices Kp and Dst from January 1st to 6th 2018.

Wave spectrograms with similar frequency profiles to those shown in Figure 1, as well as those shown in supporting material Figure S1, are commonly detected during perigee passes of the Van Allan Probes. For example, on January 2018 out of the 72 perigee passes which occurred, probe A detected 69 events with clear signatures of low frequency waves manually identified in the spectrograms. Similarly, during all of the 75 perigee passes of probe B clear wave signatures where identified. While most of the wave signatures detected during the perigee passes have the same rising and falling frequency profile some events have frequency profiles which do not fit this behavior, such as the double humped and asymmetric frequency profiles shown in some of the spectrograms presented in Figure S2 in the supporting material. During the end of the Van Allen Probe mission the perigee of the probes was lowered to altitudes <300 km. Figure S3 in the supporting material illustrates that the wave signatures can be identified in the spectrograms even during this time interval where the perigee of the probes dropped below ~300 km. Analysis of these events with more complex frequency-time profiles is beyond the scope of the current paper and will be examined in future work. However, most likely these are the signatures of changing profiles of ionospheric mass density as a result of dynamical changes to the low-L ionosphere and magnetosphere.

4. Plasma Mass Density Model

In order to investigate if the observed perturbations in the electric field are consistent with those expected from standing field line resonant oscillations of the magnetic field lines, the standing field-aligned Alfvén eigenfrequencies have been determined. The wave eigenfrequencies have been estimated using the numerical solutions to the guided toroidal Alfvén wave equation presented in Ozeke et al., 2005, (see also, Allan and Knox et. al, 1979, and Ozeke et. al., 2004). These guided toroidal Alfvén wave equations assume a dipole magnetic field and a thin sheet ionosphere. In order to determine the eigenfrequencies of the standing waves the height of the ionosphere and the Pedersen conductance need to be specified, as well as the plasma mass density along the length of the field lines (Allan and Knox et. al, 1979, and Ozeke et. al., 2005). Here, we assume an ionosphere height of 100 km and a Pedersen conductance of 10 S. However, the eigenfrequencies are only weakly dependent on the height of the ionosphere and the Pedersen conductance, with similar frequencies produced when the height of the ionosphere is $\lesssim$ 200 km, and for Pedersen conductance values $\gtrsim$ 0.1 S. The eigenfrequencies are however strongly dependent on the plasma mass density, especially near the field line apex and/or in regions of low Alfvén speed (see e.g., Ozeke et. al., 2005). The geographic latitude, longitude and altitude along the length of the magnetic field lines which the Van Allen Probe crossed during the perigee pass have been determined using the International Geomagnetic Reference Field (Thébault et. al., 2015) and the plasma mass density along the length of the magnetic field line has been determined using the empirical International Reference Ionosphere (IRI) model. The IRI models estimates the average monthly plasma mass density as a function of latitude, longitude and altitude up to a height of ~1500 km (Bilitza et. al., 1990) for magnetically quiet conditions outside of the auroral zone. The electric field spectrograms shown in Figure 2 (see also, Figure S1) appear similar during each of the perigee passes, suggesting that during January 2018 the plasma mass density along the field lines remained relatively stable. Consequently, since the mass plasma density appears stable and the geomagnetic conditions were quiet as indicated by the Kp and Dst indices shown in Figure 2, it is likely that the IRI model may give a reasonable estimate for the density along the field lines during these perigee passes.

To make progress with modeling the Alfvén eigenfrequenices along the entire field line, the plasma mass density profiles along the magnetic field lines as a function of latitude have been fitted to the function presented in equation (1).

$$y = \mathrm{a}.\,[\sin(\lambda - b)]^n + c \qquad (1)$$

Here, y represents the $\log_{10}$ of the plasma mass density, λ is the latitude of a point along the field line. The constants a, b, c and the integer constant n are selected to give the best least squares fit to the values of y and λ. The constant c gives the equatorial plasma mass density (at the apex of the field line) and b gives the latitude of the field line apex (the equatorial mid-point of the field line). Using the fitting function shown in equation (1) the plasma mass density was extrapolated to points along the field line beyond the ~1500 km altitude limit of the IRI model. An example of the plasma mass density along the field lines crossed during the perigee pass of Van Allen Probe B from 16:22 to 17:22 UTC on January 1st, 2018, is presented in Figure 3. In Figure 3 panel (a) shows the altitude versus latitude profile of the field lines crossed by the probe. Panel (b) shows the plasma mass density values along the same field lines derived from the IRI model up to an

altitude of 1500 km and the density values derived using the fitting method given by equation (1) extrapolated beyond an altitude of 1500 km.

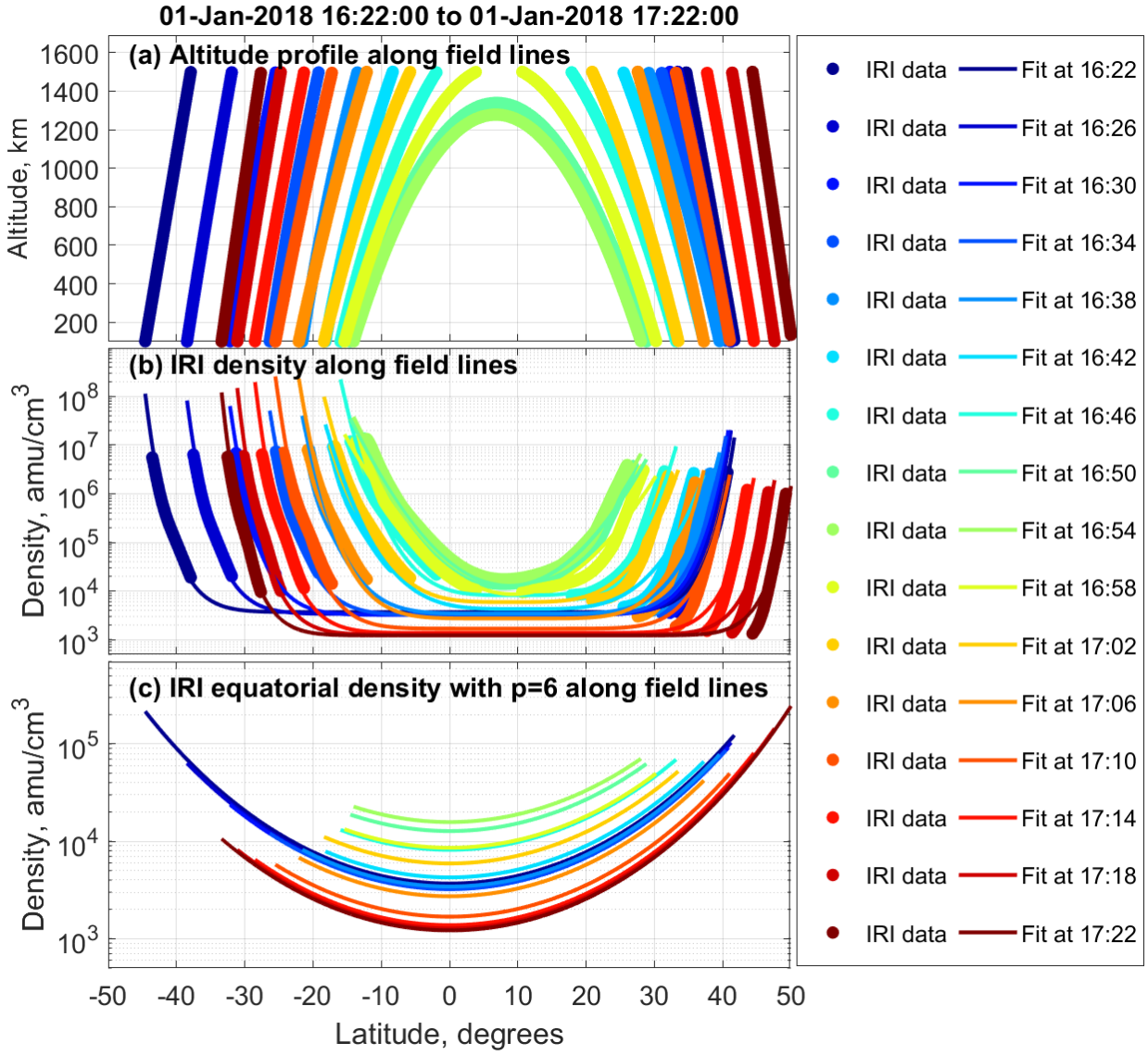

Figure 3. Panel (a) represents the plots of the altitude profile along the magnetic field lines crossed by Van Allen Probe B during the perigee pass on January 1st from 16:22 to 17:22 UTC at time intervals of 4 minutes up to a maximum height of 1500 km. Panel (b) represents the plasma mass density along the field lines shown in panel (a). The solid circles indicate plasma mass density values along the magnetic field lines obtained using the IRI model. Panel (c) represents plasma mass density profiles with the same values for equatorial density at the apex of the field line as shown in panel (b) with a density variation along the field line as given by equation (2) with p=6. Note the IRI model is valid up to a maximum altitude of 1500 km. The solid curves indicate the plasma mass density values extrapolated from the IRI model to heights beyond 1500 km using the fitting function shown in equation (1).

The standing Alfvén wave equation in a dipole field is typical solved assuming the plasma mass density along the field line varies as given by equation (2) (see, Cummings et. al., 1969, Allan & Knox et. al., 1979 and Ozeke et al., 2005).

$$\rho(\mathrm{r}) = \rho_{eq}\left(\frac{LRe}{r}\right)^{p} \quad (2)$$

Here ρ_{eq} is the equatorial plasma mass density, L is the L-shell of the field line, Re is the radius of the Earth, and r is the distance from the center of Earth to a point along the field line. Analytic solutions for the eigenfrequencies of standing toroidal Alfvén waves are only possible when the plasma density along the field varies as given by equation (2) with $p = 6$ (see, Allan and Knox, 1979). Here we examine how the model wave eigenfrequencies change when the plasma mass density along the field line varies as given by the IRI model, and when the field-aligned density is estimated more directly from the IRI model using the fits presented in equation (1) (see also Figure 3), and alternatively when the plasma mass density is assumed to vary more gradually along the field line with a field-aligned power law density profile as given by equation (2) with $p = 6$, as shown in Figure 3 (c).

5. Data-Model Comparison Results and Discussion

In Figure 4 the wave frequencies detected by probe B during the perigee pass from 16:22 to 17:22 UTC on January 1st 2018 are compared with the eigenfrequencies of standing field line resonances determined by solving the guided toroidal Alfvén wave equation. The spectrogram of the waves' electric field perturbations clearly illustrates that a discrete set of rising and falling wave frequencies occurred as the probe moved inward onto lower L-shells and then outward onto higher L-shells during this perigee pass, as shown in Figure 4 (a) (see also Figure 1). Figure 4 (b) illustrates the same spectrogram as that shown in panel (a) with the addition of the odd harmonic mode standing wave eigenfrequencies of the magnetic field lines crossed by the probe during the perigee pass overplotted. In Figure 4 (b) the plasma mass density along the length of magnetic field lines used to determine the eigenfrequencies is obtained using the IRI model and the fitting function discussed in section (4), with the mass density having the form illustrated in Figure 3 (b).

Figure 4 (b) shows that the odd harmonic mode eigenfrequencies of these standing waves are in close agreement with the discrete set of rising and falling wave frequencies detected by EFW during the perigee pass of the probe, indicating the observed wave frequencies are likely caused by odd harmonic mode standing field line resonances excited on L-shells down to L~1.1. Figure 4 (c) is similar to Figure 4 (b) except that the eigenfrequencies have been determined from analytic solutions of the guided toroidal Alfvén wave equation with a density variation along the field lines as given by equation (2) with p=6, where the mass density profiles are as illustrated in Figure 3 (c). Note that the model eigenfrequencies shown in both panels (b) and (c) of Figure 4 are determined from the guided toroidal Alfvén wave equation using the same values for the equatorial plasma mass density at the apex of the field lines given by the IRI model. Interestingly, these standing wave eigenfrequencies illustrated in panels (b) and (c) are almost identical, indicating that the eigenfrequencies are more dependent on the plasma mass density near the apex of the field

lines compared with how the density varies along the length of the field lines closer to the ionosphere.

The temporal variation in the equatorial plasma mass density used to determine the standing eigenfrequencies shown in panels (b) and (c) is illustrated in Figure 4 (d). The region in red indicates points along the perigee pass where the apex of the field lines crossed by the probe were at altitudes below 1500 km. At those points, the density can be determined entirely from the IRI model without requiring any extrapolation of the IRI densities to higher altitudes using the fitting function given by equation (1).

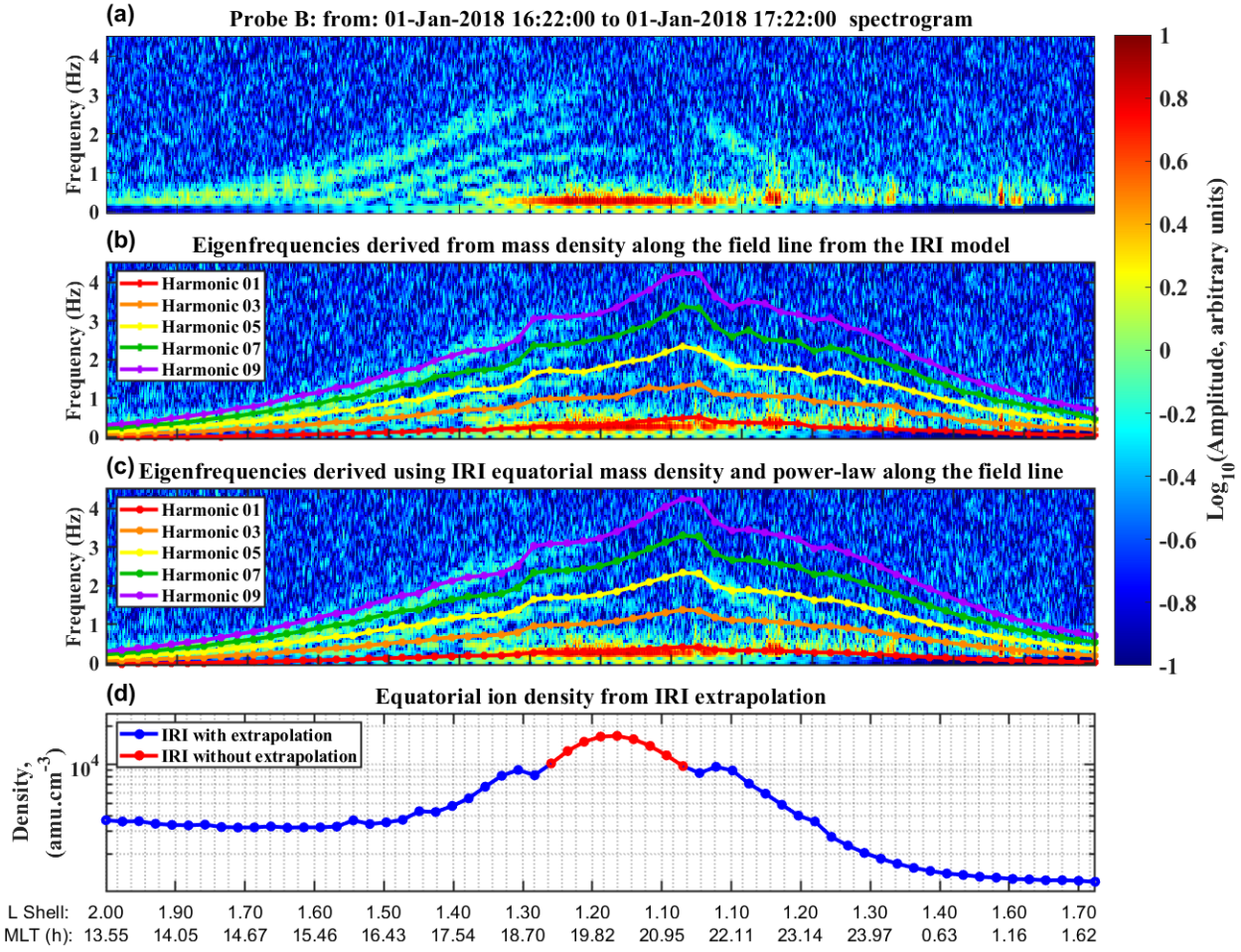

Figure 4. Panel (a) shows the electric field spectrogram during the perigee pass of probe B from 16:22 to 17:22 UTC on January 1st, 2018. Panel (b) shows the same spectrogram from panel (a) overplotted with the standing wave odd mode harmonic eigenfrequencies of the field lines crossed by probe B derived with the plasma mass density along the field line using the method discussed in section 4. Panel (c) is the same as panel (b) except the eigenfrequencies are obtained using the same equatorial plasma density as in panel (b) but the plasma density profile along the field lines is the same as that given in equation (2) with $p = 6$. Panel (d) shows the equatorial plasma mass density of the magnetic field lines crossed during the perigee pass of probe B. The

blue and red regions indicating plasma density values obtained from the IRI model with and without extrapolation respectively.

6. Conclusions

The results presented in this study show that electric field perturbations at a set of discrete wave frequencies are regularly detected by the EFW instruments at $L \lesssim 1.5$ during perigee passes of the Van Allen Probes. These waves occur at frequencies ranging from ~0.5 Hz to ~3.5 Hz, with the wave frequencies typically reaching a peak value on the lowest L-shell. The observed discrete wave frequencies are consistent with the excitation of only odd harmonic mode standing field line resonances, as validated by modeling which solves the guided toroidal Alfvén wave equation in a dipole field with plasma mass density along the field lines constrained by the IRI model. These waves appear similar to the odd harmonic mode standing guided toroidal waves detected by Van Allen Probe B, recently reported on by Takahashi et al. (2020). However, those waves occurred at much higher L-shells between dipole L-values of 4.2 and 6.1, as is commonly observed. To our knowledge, this is the first report of in-situ harmonic field line resonances with Hertz frequencies at low-L near the equator.

Our results clearly show that the eigenfrequencies of these low L-shell standing guided toroidal waves are strongly controlled by the equatorial plasma mass density at the apex of the magnetic field lines. Consequently, the regular occurrence of these standing waves offers a potentially new application of magneto-seismology for examining the dynamics of plasma mass densities in the coupled magnetosphere-ionosphere system at equatorial latitudes on very low L-shells. Inversion of the wave frequencies into density estimates could also be used for assessing the accuracy of existing plasmasphere and ionosphere models during both geomagnetically quiet and active time intervals.

Acknowledgments and Data

IRM is supported by a Discovery Grant from Canadian NSERC. This research was supported by funding from the Canadian Space Agency through a Geospace Observatory (GO) Canada Science and Applications grant. We acknowledge the WDC for Geomagnetism, Kyoto University, Japan for the geomagnetic indices (http://wdc.kugi.kyoto-u.ac.jp/). We also acknowledge use of NASA/GSFC's Space Physics Data Facility's OMNIWeb service, and OMNI data. The EFW data is available from (http://www.space.umn.edu/rbspefw-data/). The work by the EFW team was conducted under JHU/APL contract 922613 (RBSP-EFW). All data used in the paper is publically available from the links above.

References

Allan, W., & Knox, F. B. (1979). The effect of finite ionospheric conductivities on axisymmetric toroidal Alfvén wave resonances. *Planet. Space Sci.*, 939-950, doi: 10.1016/0032-0633(79)90024-2.

Anderson, B. J., Engebretson, M. J., Rounds, S. P., Zanetti, L. J., & Potemra, T. A. (1990). A statistical study of Pc 3–5 pulsations observed by the AMPTE/CCE Magnetic Fields Experiment, 1. Occurrence distributions. *Journal of Geophysical Research*, 95(A7), 10495. doi:10.1029/ja095ia07p10495.

Bilitza, D. (1990). International Reference Ionosphere. *URSI/COSPAR*, pp. NSSDC 90-22.

Chen, L., & Hasegawa, A. (1974). A theory of long-period magnetic pulsations: 1. Steady state excitation of field line resonance. *Journal of Geophysical Research,*, 79(7), 1024–1032. doi:10.1029/ja079i007p01024 .

Cummings, W. D., O'Sullivan, R. J., & Coleman, P. J. (1969). Standing Alfvén waves in the magnetosphere. *Journal of Geophysical Research*, 74(3), 778–793. doi:10.1029/ja074i003p00778.

Dent, Z. C., Mann, I. R., Goldstein, J., Menk, F. W., & Ozeke, L. G. (2006). Plasmaspheric depletion, refilling, and plasmapause dynamics: A coordinated ground-based and IMAGE satellite study. *Journal of Geophysical Research*, 111 (A3), A03205. doi: 10.1029/2005ja011046.

Engebretson, M. J., Zanetti, L. J., Potemra, T. A., & Acuna, M. H. (1986). Harmonically structured ULF pulsations observed by the AMPTE CCE Magnetic Field Experiment. *Geophysical Research Letters*, 13(9), 905–908. doi:10.1029/gl013i009p00905.

Fälthammar, C. -G. (1965). Effects of time-dependent electric fields on geomagnetically trapped radiation. *Journal of Geophysical Research*, 70(11), 2503–2516. doi:10.1029/jz070i011p02503 .

Fenrich, F. R., Samson, J. C., Sofko, G., & Greenwald, R. A. (1995). ULF high- and low-mfield line resonances observed with the Super Dual Auroral Radar Network. *Journal of Geophysical Research: Space Physics*, 100(A11), 21535–21547. doi:10.1029/95ja02024.

Fretz, K. A., Adams, E. Y., & Kirby, K. W. (2016). The Van Allen Probes Observatories: Overview and operation to date. *Johns Hopkins APL Technical Digest*, pp. vol. 33. no. 3, pp. 202–215.

Green, A. W., Worthington, E. W., Baransky, L. N., Fedorov, E. N., Kurneva, N. A., Pilipenko, V. A., & Philipov, G. V. (1993). Alfven field line resonances at low latitudes (L= 1.5). *Journal of Geophysical Research*, 98(A9), 15693. doi:10.1029/93ja00644 .

Harris, F. J. (1978). On the use of windows for harmonic analysis with the discrete Fourier transform. *Proceedings of the IEEE*, 66(1), 51–83. doi:10.1109/proc.1978.10837 .

Hasegawa, A., Tsui, K. H., & Assis, A. S. (1983). A theory of long period magnetic pulsations, 3. Local field line oscillations. *Geophysical Research Letters*, 765–767. doi:10.1029/gl010i008p00765.

Kessel, R., Fox, N., & Weiss, M. (2013). The Radiation Belt Storm Probes (RBSP) and Space Weather. *Space Sci Rev*, 179, 531–543. doi: /10.1007/s11214-012-9953-6.

Kim, H., Hwang, J., Park, J., Miyashita, Y., Shiokawa, K., Mann, I. R., Raita, T., & Lee, J. (2018). Large-scale ducting of Pc1 pulsations observed by Swarm satellites and multiple ground networks. *Geophysical Research Letters*, 45, 12,703– 12,712. https://doi.org/10.1029/2018GL080693

Kivelson, M. G., & Zu-Yin, P. (1984). The Kelvin-Helmholtz instability on the magnetopause. *Planetary and Space Science*, 32(11), 1335–1341. doi:10.1016/0032-0633(84)90077-1 .

Kletzing, C. A., Kurth, W. S., Acuna, M., MacDowall, R. J., Torbert, R. B., Averkamp, T., & Tyler, J. (2013). The Electric and Magnetic Field Instrument Suite and Integrated Science (EMFISIS) on RBSP. *Space Science Reviews 179*, 127–181. doi: 10.1007/s11214-013-9993-6.

Mathie, R. A., & Mann, I. R. (2000). Observations of an anomalously low frequency Alfvén continuum in an abnormally expanded magnetosphere. *Geophysical Research Letters*, 27(24), 4017–4020. doi:10.1029/2000gl003791 .

Mathie, R. A., Mann, I. R., Menk, F. W., & Orr, D. (1999b). Pc5 ULF pulsations associated with waveguide modes observed with the IMAGE magnetometer array. *Journal of Geophysical Research: Space Physics*, 104(A4), 7025–7036. doi:10.1029/1998ja900150.

Mathie, R. A., Menk, F. W., Mann, I. R., & Orr, D. (1999a). Discrete Field Line Resonances and the Alfvén Continuum in the Outer Magnetosphere. *Geophysical Research Letters*, 26(6), 659–662. doi:10.1029/1999gl900104.

Mauk, B. H., N. J. Fox, S. G. Kanekal, R. L. Kessel, D. G. Sibeck, and A. Ukhorskiy (2012), Science Objectives and Rationale for the Radiation Belt Storm Probes Mission, *Space Sci. Rev.*, 1–15, doi:10.1007/s11214-012-9908-y.

McIlwain, C. E. (1961). Coordinates For Mapping Distribution Of Magnetically Trapped Particles. *Journal Of Geophysical Research*, 66(11), 3681.

Menk, F. W., B. J. Fraser, C. L. Waters, C. W. S. Ziesolleck, Q. Feng, S. H. Lee, and P. W. McNabb (1994), Ground measurements of low latitude magnetospheric field line resonances, in *Solar Wind Sources of Magnetospheric Ultra-Low-Frequency Waves*, Geophys. Monogr. Ser., vol. **81**, edited by M. J. Engebreston, K. Takahashi, and M. Scholer, pp. 299–310, AGU, Washington, D. C., doi:10.1029/GM081p0299.

Ozeke, L. G., & Mann, I. R. (2001). Modeling the properties of high-mAlfvén waves driven by the drift-bounce resonance mechanism. *Journal of Geophysical Research: Space Physics*, 106(A8), 15583–15597. doi:10.1029/2000ja000393 .

Ozeke, L. G., & Mann, I. R. (2004), Modeling the properties of guided poloidal Alfvén waves with finite asymmetric ionospheric conductivities in a dipole field, *J. Geophys. Res.*, 109, A05205, doi:10.1029/2003JA010151.

Ozeke, L. G., Mann, I. R., & Mathews, J. T. (2005). The influence of asymmetric ionospheric Pedersen conductances on the field-aligned phase variation of guided toroidal and guided poloidal Alfvén waves. *J. Geophys. Res*, 110, A08210, doi:10.1029/2005JA011167.

Ozeke, L. G., Mann, I. R., Dufresne, S. K., Olifer, L., Morley, S. K., Claudepierre, S. G., & Degeling, A. W. (2020). Rapid Outer Radiation Belt Flux Dropouts and Fast Acceleration during the March 2015 and 2013 Storms: The Role of ULF Wave Transport from a Dynamic Outer Boundary. *Journal of Geophysical Research: Space Physics*, doi:10.1029/2019ja027179 .

Park, J., Lühr, H., Michaelis, I., Stolle, C., Rauberg, J., Buchert, S., & Brauer, P. (2015). Westward tilt of low-latitude plasma blobs as observed by the Swarm constellation. *Journal of Geophysical Research: Space Physics*, 120(4), 3187–3197. doi:10.1002/2014ja020965.

Rae, I. J., Donovan, E. F., Mann, I. R., Fenrich, F. R., Watt, C. E., Milling, D. K., & Balogh, A. (2005). Evolution and characteristics of global Pc5 ULF waves during a high solar wind speed interval. *Journal of Geophysical Research*, 110(A12). doi:10.1029/2005ja011007.

Ruohoniemi, J. M., Greenwald, R. A., Baker, K. B., & Samson, J. C. (1991). HF radar observations of Pc 5 field line resonances in the midnight/early morning MLT sector. *Journal of Geophysical Research: Space Physics*, 96(A9), 15697–15710. doi:10.1029/91ja00795.

Samson, J. C., Jacobs, J. A., & Rostoker, G. (1971). Latitude-dependent characteristics of long-period geomagnetic micropulsations. *Journal of Geophysical Research*, 76(16), 3675–3683. doi:10.1029/ja076i016p03675 .

Southwood, D. J. (1974). Some features of field line resonances in the magnetosphere. *Planetary and Space Science*, 22(3), 483–491. doi:10.1016/0032-0633(74)90078-6 .

Southwood, D. J., Dungey, J. W., & Etherington, R. J. (1969). Bounce resonant interaction between pulsations and trapped particles. *Planetary and Space Science*, 17(3), 349–361. doi:10.1016/0032-0633(69)90068-3 .

Srinivasan, D. K., Heyler, G. A., & McGee, T. G. (2010). Spin-Axis Estimation of the Radiation Belt Storm Probes Spacecraft using RF Doppler Data. *61st IAC (International Astronautical Congress).* Prague, Czech Republic: IAC-10-B2.6.8.

Takahashi, K., Anderson, B. J., & Strangeway, R. J. (1990). AMPTE CCE observations of Pc 3–4 pulsations at L= 2–6. *Journal of Geophysical Research*, 95(A10), 17179. doi:10.1029/ja095ia10p17179.

Thebault, E., Finlay, C. C., Beggan, C. D., Alken, P., Aubert, J., Barrois, O., Bertrand, F., Bondar, T., Boness, A., Brocco, L., Canet, E., Chambodut, A., Chulliat, A., Coisson, P., Civet, F., Du, A., Fournier, A., Fratter, I., Gillet, N., Hamilton, B., Hamoudi, M., Hulot, G., Jager, T., Korte, M., Kuang, W., Lalanne, X., Langlais, B., Leger, J.-M., Lesur, V., Lowes, F. J., Macmillan, S., Mandea, M., Manoj, C., Maus, S., Olsen, N., Petrov, V., Ridley, V., Rother, M., Sabaka, T. J., Saturnino, D., Schachtschneider, R., Sirol, O., Tangborn, A., Thomson, A., Toffner-Clausen, L., Vigneron, P., Wardinski, I., & Zvereva, T. (2015). International Geomagnetic Reference Field: the 12th generation. *Earth Planet Space*, 67, 79, doi: 10.1186/s40623-015-0228-9.

Waters, C. L., Samson, J. C., & Donovan, E. F. (1995). The temporal variation of the frequency of high latitude field line resonances. *Journal of Geophysical Research*, 100(A5), 7987. doi:10.1029/94ja02712.

Wygant, J., Bonnell, J. W., Goetz, K., Ergun, R. E., Mozer, F. S., Bale, S. D., & Harps, K. (2013). The Electric Field and Waves Instruments on the Radiation Belt Storm Probes Mission. In: Fox N., Burch J.L. (eds) The Van Allen Probes Mission. Springer, Boston, MA. https://doi.org/10.1007/978-1-4899-7433-4_6

Ziesolleck, C. W., Fraser, B. J., Menk, F. W., & McNabb, P. W. (1993). Spatial characteristics of low-latitude Pc3-4 geomagnetic pulsations. *Journal of Geophysical Research: Space Physics*, 98(A1), 197–207. doi:10.1029/92ja01433.